Buffer layer free graphene on SiC(0001) via interface oxidation in water vapor

Markus Ostler[a,b], Felix Fromm[b], Roland J. Koch[a,b], Peter Wehrfritz[a,b], Florian Speck[a], Hendrik Vita[c], Stefan Böttcher[c], Karsten Horn[c], and Thomas Seyller[b,*]

[a] Universität Erlangen-Nürnberg, Lehrstuhl für Technische Physik, Erwin-Rommel-Str. 1, D-91058 Erlangen, Germany

[b] Technische Universität Chemnitz, Institut für Physik, Reichenhainer Str. 70, D-09126 Chemnitz, Germany

[c] Max-Planck-Gesellschaft, Fritz-Haber-Institut, Faradayweg 4-6, D-14195 Berlin, Germany

Abstract: Intercalation of various elements has become a popular technique to decouple the buffer layer of epitaxial graphene on SiC(0001) from the substrate. Among many other elements, oxygen can be used to passivate the SiC interface, causing the buffer layer to transform into graphene. Here, we study a gentle oxidation of the interface by annealing buffer layer and monolayer graphene samples in water vapor. X-ray photoelectron spectroscopy demonstrates the decoupling of the buffer layer from the SiC substrate. Raman spectroscopy is utilized to investigate a possible introduction of defects. Angle-resolved photoemission spectroscopy shows that the electronic structure of the water vapor treated samples. Low-energy electron microscopy (LEEM) measurements demonstrate that the decoupling takes place without changes in the surface morphology. The LEEM reflectivity spectra are discussed in terms of two different interpretations.

1 Introduction

The growth of epitaxial graphene (EG) by thermal decomposition of SiC [1-3] at elevated temperatures in an argon atmosphere [4-5] makes high quality graphene accessible on a wafer-size scale. The growth of monolayer graphene is easily controllable [6] if SiC(0001), i.e. the Si-face, is used as a substrate. On the Si-face, the first grown carbon layer, a $(6\sqrt{3}\times6\sqrt{3})R30°$ reconstruction ($6\sqrt{3}$ for short), is covalently bound to the substrate [7]. This so-called buffer layer lacks the π bands of graphene. Only the second carbon layer has the properties of graphene. This is referred to as monolayer graphene (MLG) and resides on top the $6\sqrt{3}$ buffer layer. The buffer layer underneath MLG leads to a strong electron doping ($n \approx 1\times10^{13}$ cm^{-2}) of the latter [8-9]. Moreover, the charge carrier mobility of MLG is temperature

*Corresponding author Tel: +49 371 531-32898. E-mail: Thomas.Seyller@physik.tu-chemnitz.de (Thomas Seyller)

dependent [4] and it has been observed that this is a direct consequence of the presence of the buffer layer [10]. In recent years, various elements such as gold [11], lithium [12], silicon [13], fluorine [14], germanium [15], oxygen [16-19] and hydrogen [10, 20-23] have been intercalated between the buffer layer and SiC(0001) in order to modify the interface. Depending on the starting point, the intercalation process converts the buffer layer into monolayer graphene or monolayer graphene on top of $6\sqrt{3}$ into bilayer graphene. The non-metallic intercalants such as hydrogen, oxygen, and fluorine, are of special interest. Their strong covalent bonds to the Si atoms of the SiC surface are expected to lead to bonding and anti-bonding states far away from the Fermi energy and thus to insulating SiC surfaces. Hydrogen has been shown to work well, leading to so-called quasi-free-standing monolayer graphene (QFMLG) with improved electrical properties [10, 22-23] when compared to normal MLG which resides on the buffer layer. Hydrogen is therefore a prime candidate for the future integration of quasi-free-standing graphene into devices. Fluorine, on the other hand, has been demonstrated to lead to exceptionally high p-type doping of the resulting graphene layer with a large hole concentration of 4.5×10^{13} cm^{-2} [14].

Another interesting element for intercalation is oxygen. Oida et al. [16] have investigated the intercalation of molecular oxygen under the buffer layer using a low-temperature oxidation process (T = 250 °C, p = 1 atm, t = 5 s). They observed the formation of a 3 Å thick oxide layer below the buffer layer. Low-energy electron diffraction (LEED) revealed a weakening of the fractional order diffraction spots related the buffer layer while at the same time the first order graphene spots prevailed. From the observed π-plasmons in electron energy loss spectroscopy and graphene-related C1s core level components measured by x-ray photoelectron spectroscopy (XPS) they concluded that the buffer layer had been converted into graphene and that the latter remains undamaged by this process. Mathieu and coworkers [18] studied oxygen intercalation under MLG at higher temperature and lower oxygen pressure (T = 500 °C, p = 10^{-4} torr, t = 3 h) and concluded that the buffer layer is partially decoupled from the substrate leading to bilayer graphene on an oxidized SiC(0001) surface. We have previously compared oxygen intercalation below the $6\sqrt{3}$ buffer layer carried out under two different sets of conditions [17]. An *in-situ* high-temperature low-pressure process (T = 600 – 800 °C, p = 10^{-7} – 10^{-4} mbar, t = 30 min) was carried out inside the ultra-high vacuum chamber used for photoelectron spectroscopy. A low-temperature high-pressure process was performed *ex-situ* in a dedicated chamber (T = 200 – 270 °C, p = 100 – 1000 mbar, t = 30 min). In both cases a decoupling of the buffer layer was demonstrated by angle-resolved photoelectron spectroscopy (ARPES) and XPS. On the other hand, the ARPES

data also showed a strong broadening of the π band, signaling a considerable amount of defects, an effect that was confirmed by Raman spectroscopy. This work showed that the observation of plasmonic features, core levels, and LEED patterns alone is not sufficient to decide whether the oxygen treatment attacks graphene or not. In the work of Oliveira *et al.* [19], MLG (graphene on the buffer layer) was annealed in air at 600 °C for 40 min in order to decouple the buffer layer. The decoupling, which was unambiguously demonstrated using a variety of spectroscopic techniques (ARPES, XPS, Raman spectroscopy) led to the formation of bilayer graphene with an almost negligibly small density of defects. On the other hand, the same process carried out with buffer layer samples lead to a decoupled graphene layer with a much larger density of defects. However, since the air used in the process was not dried, the question about the role of water arises. Hence, in the present study we use pure water vapor as an oxidant, eliminating gaseous oxygen. In analogy to our previous oxidation studies [17, 19], we performed XPS to determine the decoupling of the 6√3, ARPES to study the transformation from 6√3 into graphene, and Raman spectroscopy to investigate a possible introduction of defects. Additionally, photoemission electron microscopy (PEEM) and low-energy electron microscopy (LEEM) were carried out to investigate the effect on morphology of the transition of 6√3 and MLG.

LEEM reflectivity spectra measured at intercalated samples may also increase the understanding of reflectivity spectra of epitaxial graphene on SiC. Here, a commonly accepted explanation of the dips in the reflectivity spectra [24] was recently challenged by Feenstra, Srivastava *et al.* [25-27]. The accepted interpretation was that the dips of reflectivity spectra between 0-8 eV are due to the graphite band structure in ΓA direction [24]. Since epitaxial graphene only has a few layers, the band splits into discrete energy levels. Incident electrons with a matching energy can couple to those states, which increases the transmission probability creating dips in the reflectivity curve. Thus, n minima are obtained for n layers of graphene without counting the 6√3, because of its modified of a band structure [7]. In contrast, Feenstra and co-workers [25-26] claim that inter-layer states between graphene layers are responsible for the dips. The interpretation gives rise to n-1 dips for n graphene layers, however, this time counting the 6√3 because it is *graphene-like*. Of course, for graphene on SiC(0001), the results are the same if n dips are matched to n graphene layers or n-1 dips are matched to n carbon layers including the 6√3. Results, however, strongly differ after conversion of the buffer layer to graphene which we will discuss in this work.

2 Experimental aspects

The 6H-SiC substrate material used in the present study was purchased from *SiCrystal*. Samples were cut from the wafer and cleaned by a wet chemical procedure described elsewhere [28]. Prior to the growth of the buffer layer or of graphene, the samples were etched in hydrogen in order to remove polishing damages [6]. In order to grow the buffer layer and MLG, the substrates were annealed for 15 min in 1 bar of Ar at temperatures of 1475 and 1675 °C, respectively, using a custom-built reactor described earlier [6].

Water vapor treatment was performed in a dedicated vacuum chamber. In order to produce an oxygen free atmosphere, deionized water was placed in a reservoir inside the chamber and frozen by evacuating with high pumping speed. After reaching a base pressure of ~10^{-3} mbar, the valve to the pump was closed. Subsequently, the ice was allowed to melt and to warm up to room temperature leading to a saturated water vapor atmosphere of approximately 28 mbar. Heating of the sample was accomplished with the help of a conductive heater. The sample temperature, which was measured by a thermocouple, was held constant for 30 min at 500 and 650 °C for the treatment of buffer layer and MLG samples, respectively. That the intercalation of water under MLG requires a somewhat higher annealing temperature is most likely due to the diffusive nature of the process. The preparation conditions are compiled in Table 1.

Starting sample type	Ar annealing			Water treatment			Resulting sample type
	T/°C	*p*/mbar	*t*/min	*T*/°C	*p*/mbar	*t*/min	
Buffer layer (6√3)	1475	1000	15	500	~28	30	Decoupled monolayer graphene
Monolayer graphene (MLG)	1675	1000	15	650	~28	30	Decoupled bilayer graphene

Table 1. Conditions for the growth of buffer layer and MLG in Ar, as well as for the treatment of the samples in water vapor.

Several buffer layer and MLG samples were annealed in water vapor. All samples were characterized by means of XPS to ensure complete decoupling of the 6√3. In addition, those samples were investigated by Raman spectroscopy, ARPES or LEEM. To provide freshly prepared samples for each investigation, different but comparable samples were used for Raman spectroscopy, ARPES and LEEM. XPS was carried out with a monochromated Al-K_α X-ray source and a hemispherical energy analyzer *SPECS* Phoibos 150. A *Jobin Yvon* T64000 triple spectrometer was utilized for micro-Raman measurements under ambient conditions in a confocal backscattering geometry. Using a 100x objective, a frequency doubled Nd:YVO_4 laser with a wavelength of 532 nm was focused on the sample for excitation. ARPES data were taken using a *SPECS* Phoibos 100 analyzer at beam line UE56-

2/PGM-1 of the storage ring BESSY II. PEEM images, LEEM images and reflectivity curves were recorded by a *SPECS* FE-LEEM P90 system.

3 Results and Discussion

Fig. 1 shows XPS measurements of the buffer layer ($6\sqrt{3}$) and MLG before and after annealing in water vapor. The buffer layer C1s core level spectrum in Fig. 1a can be deconvoluted in three symmetric components [7]. The component labeled SiC at (283.85 ± 0.05) eV originates from the substrate. The two signals S1 and S2 at (285.0 ± 0.1) eV and (285.65 ± 0.05) eV, respectively, are due to carbon atoms of the buffer layer. Here, S2 stems from atoms bound only in-plane and S1 from atoms additionally bound to the substrate [7]. In the case of MLG, the carbon atoms of the graphene layer residing on top of the buffer layer add an asymmetric component at (284.7 ± 0.05) eV which we denote by G in Fig. 1b. After annealing the buffer layer in water vapor, the spectrum in Fig. 1c exhibits only two components: the signal of the substrate at (282.55 ± 0.05) eV and an asymmetric component labeled by G at (284.25 ± 0.05) eV, which has similar shape and intensity as the G component of MLG. With the buffer layer components missing and a graphene like component arising upon annealing in water vapor, this is a strong indication that the buffer layer becomes decoupled from the substrate and transforms into decoupled graphene as is the case when annealing the buffer layer in hydrogen [20-21]. MLG also exhibits two components after water vapor treatment (see Fig. 1d). The substrate signal lies at (282.9 ± 0.05) eV and the component G at (284.25 ± 0.05) eV. The G component is larger compared to the water-treated buffer layer sample, because the atoms of the buffer layer transformed into graphene add to the signal of the graphene atoms already present before treatment. These results show that C1s core level spectra of buffer layer and MLG annealed in water vapor have a strong resemblance to buffer layer and MLG annealed in hydrogen [21].

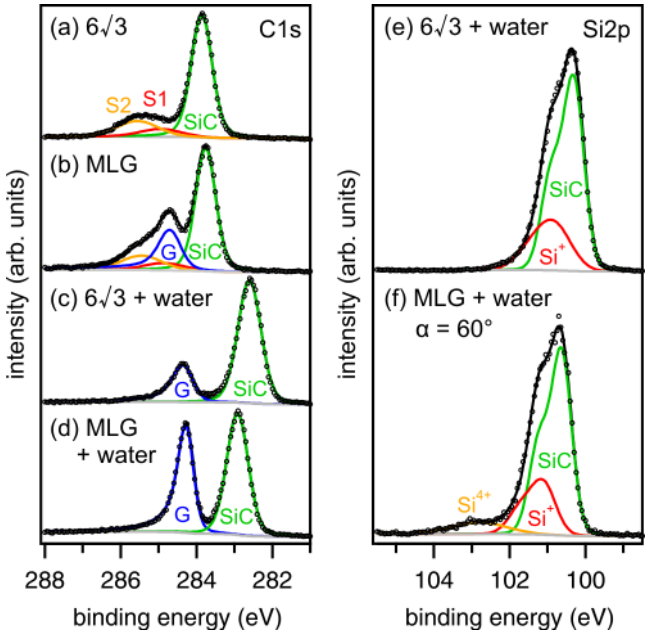

Fig. 1. C1s core level spectra of (a) pristine buffer layer, (b) pristine MLG, (c) water-treated buffer layer, and (d) water-treated MLG. Si2p core level spectra of (e) water-treated buffer layer and (f) water-treated MLG. Spectra are offset for clarity and except (f) all were taken at normal emission; (f) at 60° emission angle.

The Si2p core level of the buffer layer (6√3) after water treatment (Fig. 1e) contains two components. To model the line shape, we used Voigt doublets to account for the spin-orbit splitting in the Si2p core level. Apart from the substrate component SiC at (100.31 ± 0.05) eV, there is an additional component at (100.79 ± 0.1) eV, which we assign to Si^+, because of its typical chemical shift of 0.5 eV with respect to the SiC component [29]. When the water treatment is applied to MLG (Fig. 1f), there is an additional small component at (102.61 ± 0.05) eV with a chemical shift typical of Si^{4+} [29]. The only elements found in a wide energy spectrum (not shown) for treated 6√3 and MLG were C, Si, and O. Therefore, Si^+ can be attributed to C_3-Si-O, i.e. to a silicon atom of the topmost SiC bilayer bound to a single oxygen atom. The Si^{4+} signal originates from a very thin layer (≤ 1 monolayer) of SiO_2 which apparently is only formed in the case of treated MLG. We believe that this is a result of the somewhat increased process temperature which was needed to intercalate the water under two carbon layers.

Upon annealing in water vapor, the substrate components shift towards lower binding energy. The shift is the same for the C1s and Si2p core levels and amounts to 1.2 eV for buffer layer (6√3) and 0.9 eV for MLG. It is caused by a variation of the Fermi level position with respect to the SiC band edges, i.e. a change in the surface band bending. The difference in the amount of the shift for 6√3 and MLG is likely to arise from the different interface which is reflected by the absence and presence of SiO_2. The oxidation of the SiC interface

implies that at least part of the intercalated water was decomposed to be used as an oxygen source. No evidence was found suggesting that molecular water remained between the oxide layer and the graphene layers. The absence of molecular water was potentially due to the high processing temperature of 500 °C and 650 °C. In contrast, Kim et al. [30] observed a layered structure of water monolayers between graphene and mica after water intercalation at room temperature.

Raman spectroscopy was performed to investigate a possible damage introduced by the water vapor treatment. It also allows the unambiguous identification of graphene. Fig. 2 shows the Raman spectrum of the buffer layer (bottom) and MLG (middle) after annealing in water vapor. For comparison, there is a spectrum of MLG annealed in hydrogen (top), also known as quasi-free-standing bilayer graphene (QFBLG). The water-treated buffer layer exhibits a G and 2D line as expected for graphene. However, there are also high intensities of the defect related D, D' and D+D' lines. From the ratio of the G and D intensities (I(D)/I(G)) we can estimate the average distance between defects to be 7 nm [31]. The I(D)/I(D') ratio can be used to classify the type of defect. Eckmann *et al.* [32] report a I(D)/I(D') ratio of 7 for vacancy-like defects and 13 for sp^3 hybridization. For water treated $6\sqrt{3}$ we determine the ratio to be 8.4. This means that the treated buffer layer exhibits vacancy-like defects being consistent with the XPS C1s spectrum in Fig. 1c, which shows – apart from the SiC substrate – no signs for sp^3 hybridization of carbon atoms in the form of C-O or Si-C bonds. The results described above are in perfect agreement with our previous work on oxygen intercalation underneath the buffer layer [17]. The Raman spectrum of water-treated MLG (center of Fig. 2) reveals that the sample is almost defect-free as it shows only a small bump in the region of the D line, similar to high quality QFBLG (top spectrum). The 2D line is asymmetric and can be fitted with four components indicating bilayer graphene [33]. Due to the high defect densities introduced by the water vapor treatment of the buffer layer, intercalation of water vapor is not considered an improvement over the intercalation of oxygen. Thus, intercalation of hydrogen [20] still remains the most promising method to obtain quasi-free-standing monolayer graphene through intercalation. In contrast, annealing MLG in water vapor yields almost defect-free bilayer graphene, very similar to the annealing of MLG in air [19]. Raman spectroscopy analysis suggests that annealing in water vapor instead of hydrogen is a promising alternative method to obtain quasi-free-standing bilayer graphene.

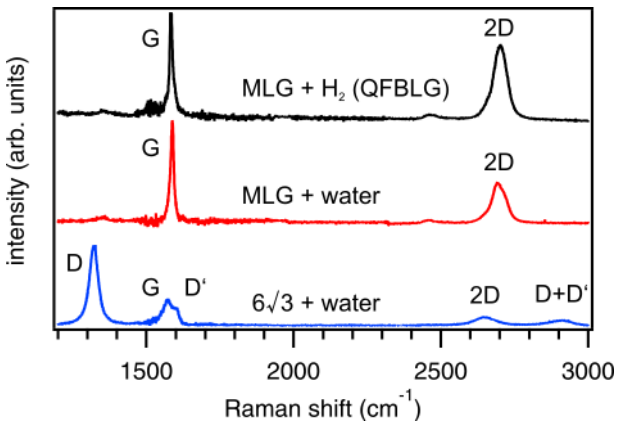

Fig. 2. Raman spectra of MLG (center) and buffer layer (6√3) (bottom) after water treatment and MLG after annealing in hydrogen (top) for comparison. Wavelength of excitation laser was 532 nm. For clarity spectra are offset in intensity.

ARPES reveals the changes in the electronic structure of water-treated buffer layer and MLG. Fig. 3 shows the measured valence band features for (a) water-treated buffer layer and (c) water-treated MLG in two high symmetry directions: ΓMΓ on the left side and ΓKM on the right. In Fig. 3a, the sharp π band with a local maximum at the M point and a linear dispersion in the vicinity of the K point can clearly be seen. This is typical of monolayer graphene and indicates the transformation of the buffer layer into decoupled graphene, which is consistent with the XPS and Raman spectra. Measurements close to the K point perpendicular to the ΓKM direction, in the so-called KK direction, show both sides of the Dirac cone (Fig. 3b). Extrapolation of the bands places the Dirac point (0.25 ± 0.03) eV above the Fermi energy. This is consistent with the position of the C1s core level of (284.25 ± 0.05) eV and indicates a hole concentration on the order of 4.5×10^{12} cm^{-2}. Hall effect measurements resulted in a hole concentration of 8×10^{12} cm^{-2}, which is somewhat larger but still consistent with the photoemission data. At this concentration, the room temperature charge carrier mobility is 420 cm^2/Vs which is reasonably high if we consider the high defect density seen in Raman spectroscopy. It is interesting to note that those defects apparently have only little impact on the sharpness of the bands measured in ARPES at room temperature.

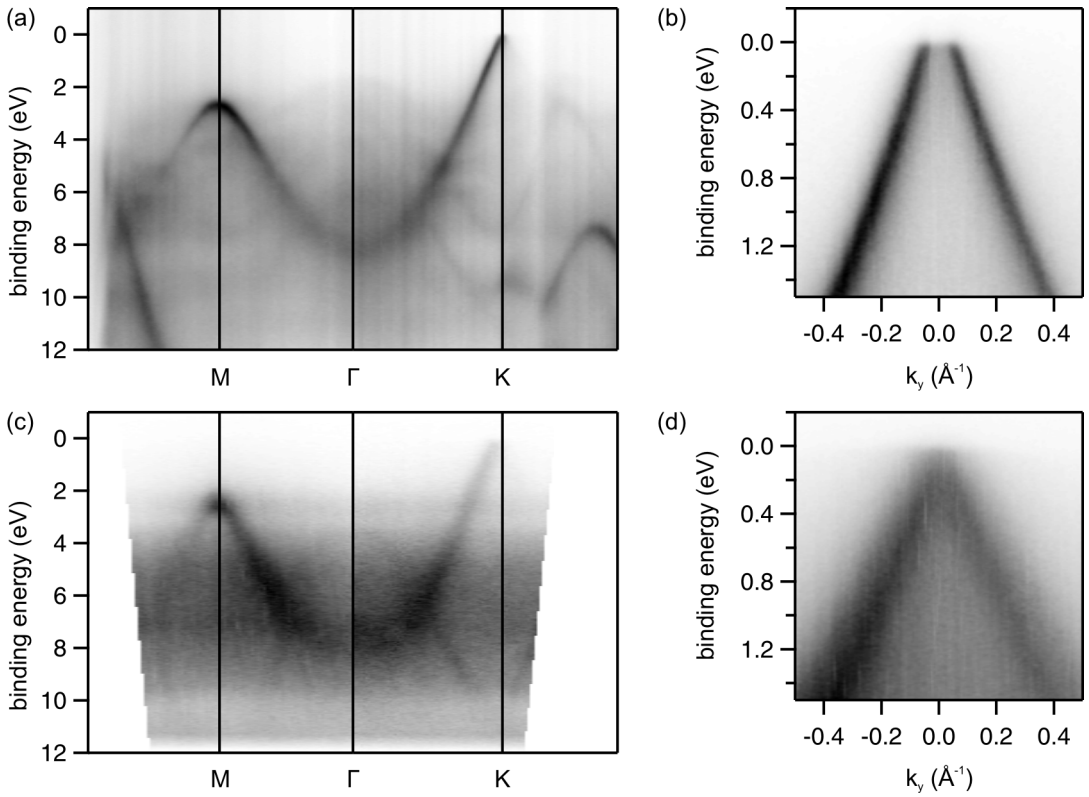

Fig. 3. ARPES band structure measured at 70 eV photon energy in ΓMΓ and ΓKM direction of (a) buffer layer and (c) monolayer graphene treated with water vapor. (b) and (d) show detail measurements in the vicinity of the K point in KK direction, corresponding to (a) and (c), respectively.

In the case of water-treated MLG, the graphene-like π band is clearly visible in Fig. 3c but the bands are much broader and there is a considerably higher background than in the case of the water-treated buffer layer. Note that the background is very high in the energy window between approximately 5 and 10 eV. Previous studies of oxidized SiC surfaces [34-37] have shown that O2p states exhibit binding energies which fall in that region. Virojanadara and Johansson have observed a large density of states between 5 and 10 eV binding energy [37] for oxidized SiC(0001). In the case of ordered silicate adlayer structures on hexagonal SiC{0001} surfaces, the O2p-Si(3s,3p) bonding states were observed at a binding energy of around 9 – 11 eV with respect to the SiC valence band maximum, while the O2p lone pair states were found at around 6 eV . Hence we associate the diffuse intensity in the ARPES data between 5 and 10 eV with the valence band states of the thin oxide layer formed during water-treatment of MLG. The apparent broadening of the π band is due to inhomogeneities of the sample surface, either from a nonuniform graphene coverage or from doping of the oxide layer. As stated above, the average thickness of that layer is less than one monolayer which translates into a partial coverage of the surface. As a consequence of the inhomogeneous coverage with SiO_2 the doping of the graphene bilayer on top of it is much likely

inhomogeneous which could explain the broadening of the bands. This is supported by the fact that in the case of the water-treated buffer layer where no SiO_2 was observed, the bands are narrower despite a large D-line occurring in the Raman spectrum. Apparently, the broadening of the bands cannot be directly taken as evidence for defects.

Fig. 3d shows the π bands of water-treated MLG in the vicinity of the K point. In contrast to previous work [19] on annealing MLG in air, we were not able to resolve the individual π bands in ARPES arising from the formation of a bilayer. This might be due to the limited resolution induced by the disordered SiO_2 layer. Also, the exact position of the Dirac point is hard to determine but it is apparent that it is not far away from the Fermi level. The C1s core level was observed at (284.25 ± 0.05) eV which suggests a hole concentration of the order of 10^{13} cm^{-2}. Hall effect measurements performed under ambient conditions show a p-type carrier concentration of $2 \cdot 10^{13}$ cm^{-2}. The reason for this discrepancy is presently unknown. A plausible reason may be that additional p-type doping is induced by residual photo resist used for device patterning. Taking the high carrier concentration into account, the measured mobility of 790 cm^2/Vs is quite promising.

In order to further investigate the process and the morphological properties of the water-treated buffer layer and MLG, the samples were studied by LEEM and PEEM. Fig. 4a and Fig. 4b show PEEM images of a $6\sqrt{3}$ sample before and after water treatment. The images were taken from the same sample position under UV illumination from a Hg-lamp and without an electron energy filter. In this setup, the contrast is determined mainly by differences in the work function ϕ [38]. During growth of the $6\sqrt{3}$, it is possible that MLG forms at the SiC step edges. The light gray areas in Fig. 4a correspond to $6\sqrt{3}$ which has a lower ϕ of 3.75 eV [39] and the dark gray areas to MLG which has a higher ϕ of 4.33 eV [39]. In the lower part of the image, two screw dislocations in the SiC substrate are visible which dominate the SiC step structure. The feature in the top right corner is the end of a mark, which was carved into the sample before the wet chemical cleaning to assist in sample positioning. From Fig. 4b, it is clear that the overall surface morphology is unchanged by the water vapor treatment, which is no surprise considering the low process temperature of 500 °C. However, the contrast of the image is inverted. XPS suggests that MLG is not transformed at a process temperature of 500 °C. This means that the areas which appear in light gray in Fig. 4b can still be assigned to MLG. Thus, the inverted contrast shows that intercalation changes the work function of the $6\sqrt{3}$ areas from a value lower than MLG to a value higher than MLG, i.e. at least by 0.6 eV.

Bright field LEEM images were also taken before (Fig. 4c) and after (Fig. 4d) water treatment. The shown images were acquired with an electron energy of 1.0 and 6.2 eV, respectively. Each of them is part of a larger set of images which were taken with energies spanning a larger range. The set of images allows the extraction of reflectivity spectra for every pixel. The spectra averaged over the dashed and solid rectangles are plotted in Fig. 4e with corresponding lines. As reported before in Ref. [24], the reflectivity curve of the 6√3 (dashed line) is relatively flat. In contrast, the spectrum of water-treated 6√3 exhibits two dips, which will be discussed below.

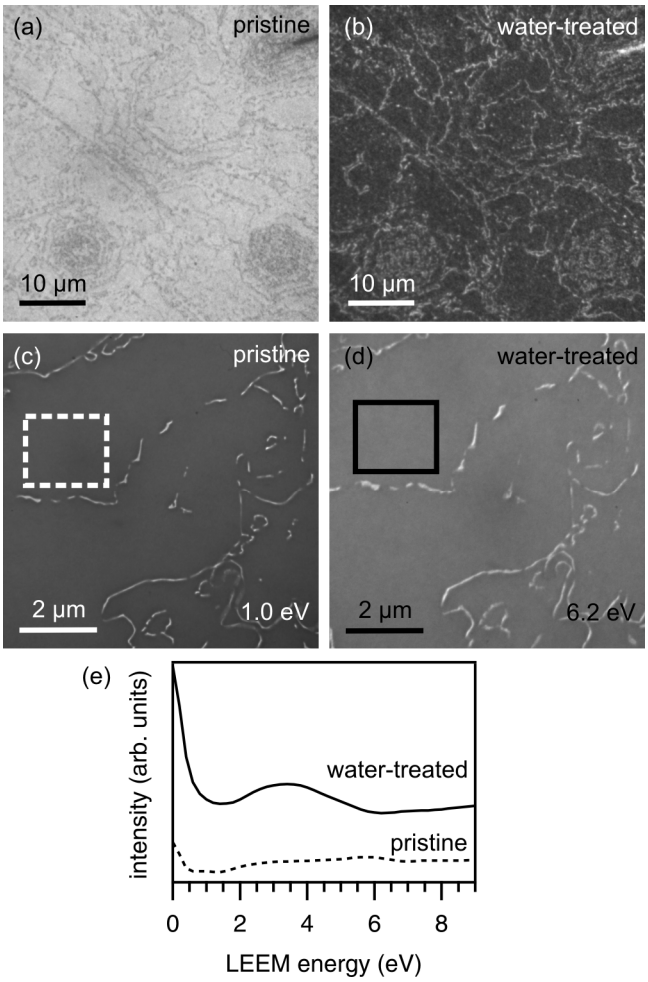

Fig. 4. PEEM images of (a) pristine and (b) water-treated buffer layer taken with Hg-lamp excitation and without energy filter to image work function differences. Bright field LEEM images (c) and (d) show buffer layer before and after water treatment at 1.0 and 6.2 eV, respectively. Spectra recorded in the dashed and solid rectangles are plotted in (e) with corresponding lines.

Fig. 5 shows bright field images from the same area a nominal MLG sample with a unusual high graphene coverage before (Fig. 5a) and after (Fig. 5b) water treatment. Note, that this sample was not identical to the one used for the Raman spectroscopy and ARPES

investigations, which had a lower graphene coverage. The LEEM images shown were acquired with an electron energy of 4.6 eV. In analogy to the 6√3 sample above, reflectivity spectra were extracted for every pixel. Four typical (standard) spectra A-D and E-H, respectively, for each image are shown in Fig. 5c and 5d. A comparison of the spectra extracted for each pixel with the standard spectra was used to obtain the false color images in Fig. 5e and 5f. When we compare the false color images before and after treatment, we can unambiguously match the reflectivity curves before and after treatment; A, B, C, D to E, F, G, H, respectively.

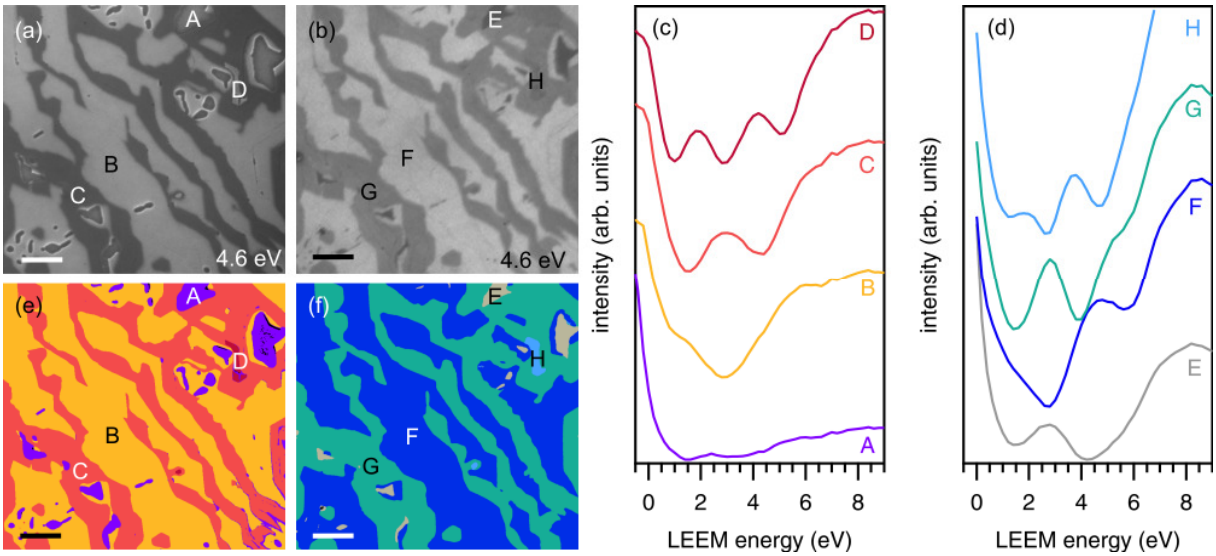

Fig. 5. Bright field LEEM images taken at 4.6 eV of (a) pristine and (b) water vapor treated MLG. Letters A-H indicate where the corresponding reflectivity spectra shown in (c) and (d) were taken. False color images (e) and (f) were generated by comparing the spectrum of every pixel with the standard spectra shown in (c) and (d). Length of the scale bar is 1 µm.

Before water treatment, the assignment of the number of graphene layers to the number of dips in the corresponding reflectivity curves is independent of their interpretation by Hibino *et al.* [24] or Feenstra *et al.* [25], because there is still a buffer layer. Thus, we can unambiguously match the colored areas in Fig. 5e to a graphene thickness. We assign purple areas (A) to buffer layer, orange areas (B) to MLG, regions in light red (C) to bilayer graphene (BLG), and the small region in dark red (D) to trilayer graphene (TLG). A total coverage of 1.3 ML can be extracted from the false color image. The regions with different coverage allow studying the behavior of LEEM spectra for a variety of thicknesses at the same time.

As above, the surface morphology is also unchanged by the water vapor treatment at a process temperature of 650 °C. However, the buffer layer areas of the pristine sample (purple

(A) in Fig. 5e) appear larger than the corresponding areas after water treatment (grey (E) in Fig. 5f). This is an artifact caused by the large difference between the work function of buffer layer and MLG, which is so high that it is not possible to focus on both buffer layer and MLG at the same time. As a consequence, the buffer layer regions become blurred and appear larger when the system is focused on MLG. After water treatment, when the buffer layer is converted into graphene, the work function difference is reduced and both regions can be sharply imaged at the same time.

The reflectivity curve of water treated buffer layer (E) is similar to the one plotted in Fig. 4e. Both exhibit two dips, and both spectra have a dip at 1.4 eV, although the energy of the second dip is different. For a 6√3 sample processed in water vapor at 500 °C (Fig. 4e), the second dip lies at 6.0 eV, while water-treated 6√3 regions found on a MLG sample processed at 650 °C (Fig. 5d, curve E) show the dip at 4.2 eV. As discussed above, they differ in their interfaces, as one (650 °C) has a SiO_2 layer, which the other (500 °C) lacks. Thus, the shift in energy of this dip strongly suggests that it originates from the interface. Indeed, this conclusion was also drawn in the studies of 6√3 intercalated by H [40] and by Ge [15], where also two dips are evident in the reflectivity curves. In both references the lower energy dip was associated with the formation of monolayer graphene. At first glance, this seems to raise a contradiction with the interpretation of Feenstra *et al.* [25]. If the dips are caused by inter-layer states between carbon layers (including the 6√3), transformation of the 6√3 to monolayer graphene should not yield an extra dip. The explanation, which is discussed in detail in ref. [27] is that decoupling of the 6√3 allows inter-layer states to form between the substrate and the former 6√3. In the case of water-treated 6√3, the distance between the substrate and the graphene layer seems to be large enough that two inter-layer states are seen in the energy range of the reflectivity spectrum, leading to two dips.

For water-treated MLG regions, we also note two dips in the reflectivity curve (F); a dip at about 2.8 eV which was also present before water treatment and an additional dip at 5.8 eV. In the case of the treated bilayer area, this additional feature is observed as a shoulder at the same energy in spectrum (G), while the two dips associated with bilayer graphene at 1.5 and 4.4 eV are still present, although somewhat shifted at 1.5 and 4.0 eV. This behavior can also be explained on the basis of the interpretation by Feenstra *et al.* [25]. Transforming monolayer graphene on top of 6√3 into quasi-free-standing bilayer graphene, or bilayer graphene on top of 6√3 into quasi-free-standing trilayer graphene does not change the inter-layer states between the carbon layers. This is the reason why dips typical of monolayer and bilayer graphene are preserved. The additional dip is again explained by the decoupling of the

6√3 from the substrate. For trilayer graphene we see no significant difference in the spectra D and H. However, XPS cannot determine if the buffer layer below trilayer regions is decoupled, since those regions amount to only a small fraction of the surface.

4 Conclusions

We demonstrate that water vapor is a good oxidant being able to passivate the SiC interface in a controlled process in the absence of gaseous oxygen. For both buffer layer and MLG, water treatment oxidizes the interface and decouples the buffer layer. In the case of 6√3, this leads to quasi-free-standing monolayer graphene, albeit with a significant amount of defects comparable to our previous work on oxygen intercalation of 6√3 [17]. MLG being more inert endures water vapor treatment at even higher temperatures without introducing defects. XPS and Raman spectroscopy confirm the transformation of MLG to bilayer graphene. ARPES cannot resolve the two π bands, most likely because of the underlying SiO_2 layer. LEEM, PEEM and reflectivity curves also give evidence for the intercalation and decoupling of the 6√3. Our observations support a recent re-interpretation of LEEM reflectivity spectra by Feenstra *et al.* [25-26] and Srivastava *et al.* [27].

Acknowledgements

This work has been supported by the European Science Foundation (ESF) under the EUROCORES Program EuroGRAPHENE CRP GRAPHIC-RF and CRP SpinGraph, by the DFG in the framework of PRIORITY PROGRAM 1459 GRAPHENE, and by the European Union through the project Concept Graphene (FP7 grant agreement n°257829).

References

[1] Berger C, Song Z, Li T, Li X, Ogbazghi AY, Feng R, et al. Ultrathin Epitaxial Graphite: 2D Electron Gas Properties and a Route toward Graphene-based Nanoelectronics. J Phys Chem B. 2004;108:19912-6.

[2] Berger C, Song Z, Li X, Wu X, Brown N, Naud C, et al. Electronic confinement and coherence in patterned epitaxial graphene. Science. 2006;312:1191-6.

[3] First PN, de Heer WA, Seyller T, Berger C, Stroscio JA, Moon J-s. Epitaxial Graphenes on Silicon Carbide. MRS Bull. 2011;35:296-305.

[4] Emtsev KV, Bostwick A, Horn K, Jobst J, Kellogg GL, Ley L, et al. Towards wafer-size graphene layers by atmospheric pressure graphitization of silicon carbide. Nat Mater. 2009;8(3):203-7.

[5] Virojanadara C, Syväjarvi M, Yakimova R, Johansson L, Zakharov AA, Balasubramanian T. Homogeneous large-area graphene layer growth on 6H-SiC(0001). Phys Rev B. 2008;78:245403.

[6] Ostler M, Speck F, Gick M, Seyller T. Automated preparation of high-quality epitaxial graphene on 6H-SiC(0001). Phys Status Solidi B. 2010;247(11-12):2924-6.

[7] Emtsev KV, Speck F, Seyller T, Ley L. Interaction, growth, and ordering of epitaxial graphene on SiC{0001} surfaces: A comparative photoelectron spectroscopy study. Phys Rev B. 2008;77:155303.

[8] Deretzis I, La Magna A. Role of covalent and metallic intercalation on the electronic properties of epitaxial graphene on SiC(0001). Phys Rev B. 2011;84:235426.

[9] Kopylov S, Tzalenchuk A, Kubatkin S, Fal'ko VI. Charge transfer between epitaxial graphene and silicon carbide. Appl Phys Lett. 2010;97:112109.

[10] Speck F, Jobst J, Fromm F, Ostler M, Waldmann D, Hundhausen M, et al. The quasi-free-standing nature of graphene on H-saturated SiC(0001). Appl Phys Lett. 2011;99(12):122106.

[11] Premlal B, Cranney M, Vonau F, Aubel D, Casterman D, De Souza MM, et al. Surface intercalation of gold underneath a graphene monolayer on SiC(0001) studied by scanning tunneling microscopy and spectroscopy. Appl Phys Lett. 2009;94(26):263115.

[12] Virojanadara C, Watcharinyanon S, Zakharov AA, Johansson LI. Epitaxial graphene on 6H-SiC and Li intercalation. Phys Rev B. 2010;82(20):205402.

[13] Xia C, Watcharinyanon S, Zakharov AA, Yakimova R, Hultman L, Johansson LI, et al. Si intercalation/deintercalation of graphene on 6H-SiC(0001). Phys Rev B. 2012;85(4):045418.

[14] Walter AL, Jeon K-J, Bostwick A, Speck F, Ostler M, Seyller T, et al. Highly p-doped epitaxial graphene obtained by fluorine intercalation. Appl Phys Lett. 2011;98:184102.

[15] Emtsev KV, Zakharov AA, Coletti C, Forti S, Starke U. Ambipolar doping in quasifree epitaxial graphene on SiC(0001) controlled by Ge intercalation. Phys Rev B. 2011;84(12):125423.

[16] Oida S, McFeely FR, Hannon JB, Tromp RM, Copel M, Chen Z, et al. Decoupling graphene from SiC(0001) via oxidation. Phys Rev B. 2010;82(4):041411.

[17] Ostler M, Koch RJ, Speck F, Fromm F, Vita H, Hundhausen M, et al. Decoupling the Graphene Buffer Layer from SiC(0001) via Interface Oxidation. Mater Sci Forum. 2012;717-720:649-52.

[18] Mathieu C, Lalmi B, Menteş TO, Pallecchi E, Locatelli A, Latil S, et al. Effect of oxygen adsorption on the local properties of epitaxial graphene on SiC (0001). Phys Rev B. 2012;86(3):035435.

[19] Oliveira MH, Schumann T, Fromm F, Koch R, Ostler M, Ramsteiner M, et al. Formation of high-quality quasi-free-standing bilayer graphene on SiC(0001) by oxygen intercalation upon annealing in air. Carbon. 2013;52:83-9.

[20] Riedl C, Coletti C, Iwasaki T, Zakharov AA, Starke U. Quasi-Free-Standing Epitaxial Graphene on SiC Obtained by Hydrogen Intercalation. Phys Rev Lett. 2009;103:246804.

[21] Speck F, Ostler M, Röhrl J, Jobst J, Waldmann D, Hundhausen M, et al. Quasi-Freestanding Graphene on SiC(0001). Mater Sci Forum. 2010;645-648:629-32.

[22] Robinson JA, Hollander M, LaBella M, Trumbull KA, Cavalero R, Snyder DW. Epitaxial Graphene Transistors: Enhancing Performance via Hydrogen Intercalation. Nano Lett. 2011;11(9):3875-80.

[23] Tanabe S, Takamura M, Harada Y, Kageshima H, Hibino H. Quantum Hall Effect and Carrier Scattering in Quasi-Free-Standing Monolayer Graphene. Appl Phys Express. 2012;5(12):125101.

[24] Hibino H, Kageshima H, Maeda F, Nagase M, Kobayashi Y, Yamaguchi H. Microscopic thickness determination of thin graphite films formed on SiC from quantized oscillation in reflectivity of low-energy electrons. Phys Rev B. 2008;77:075413.

[25] Feenstra RM, Srivastava N, Gao Q, Widom M, Diaconescu B, Ohta T, et al. Low-energy electron reflectivity from graphene. Phys Rev B. 2013;87:041406.

[26] Feenstra RM, Widom M. Low-energy electron reflectivity from graphene: First-principles computations and approximate models. Ultramicroscopy. 2013;130:101-8.

[27] Srivastava N, Gao Q, Widom M, Feenstra RM, Nie S, McCarty KF, et al. Low-energy electron reflectivity of graphene on copper and other substrates. Phys Rev B. 2013;87:245414.

[28] Sieber N, Seyller T, Graupner R, Ley L, Mikalo R, Hoffmann P, et al. Wetchemical preparation of silicate adlayer terminated SiC(0001) surfaces studied by PES and LEED. Mater Sci Forum. 2002;389-393:717-20.

[29] Sieber N, Seyller T, Graupner R, Ley L, Mikalo R, Hoffmann P, et al. PES and LEED study of hydrogen- and oxygen-terminated 6H–SiC(0001) and (000-1) surfaces. Appl Surf Sci. 2001;184:278-83.

[30] Kim J-S, Choi JS, Lee MJ, Park BH, Bukhvalov D, Son Y-W, et al. Between scylla and charybdis: hydrophobic graphene-guided water diffusion on hydrophilic substrates. Sci Rep. 2013;3:2309.

[31] Cançado LG, Jorio A, Ferreira EHM, Stavale F, Achete CA, Capaz RB, et al. Quantifying Defects in Graphene via Raman Spectroscopy at Different Excitation Energies. Nano Lett. 2011;11:3190-6.

[32] Eckmann A, Felten A, Mishchenko A, Britnell L, Krupke R, Novoselov KS, et al. Probing the nature of defects in graphene by Raman spectroscopy. Nano Lett. 2012;12:3925-30.

[33] Röhrl J, Hundhausen M, Emtsev KV, Seyller T, Graupner R, Ley L. Raman spectra of epitaxial graphene on SiC(0001). Appl Phys Lett. 2008;92:201918.

[34] Hollering M, Maier F, Sieber N, Stammler M, Ristein J, Ley L, et al. Electronic states of an ordered oxide on C-terminated 6H-SiC. Surf Sci. 1999;442(3):531-42.

[35] Hollering M, Sieber N, Maier F, Ristein J, Ley L, Riley JD, et al. Electronic and Atomic Structure of an Ordered Silicate Adlayer on Hexagonal SiC. Mater Sci Forum. 2000;338-342:387-90.

[36] Sieber N, Hollering M, Ristein J, Ley L. Photoemission Study of the Silicate Adlayer Reconstruction on Si-terminated 6H-SiC (0001). Mater Sci Forum. 2000;338-342:391-4.

[37] Virojanadara C, Johansson LI. Oxidation studies of 4H-SiC(0001) and (0001). Surf Sci. 2002;505(1-3):358-66.

[38] Bauer E, Mundschau M, Swiech W, Telieps W. Surface studies by low-energy electron microscopy (LEEM) and conventional UV photoemission electron microscopy (PEEM). Ultramicroscopy. 1989;31:49-57.

[39] Mattausch A, Pankratov O. Ab Initio Study of Graphene on SiC. Phys Rev Lett. 2007;99:076802.

[40] Forti S, Emtsev KV, Coletti C, Zakharov AA, Riedl C, Starke U. Large-area homogeneous quasifree standing epitaxial graphene on SiC(0001): Electronic and structural characterization. Phys Rev B. 2011;84:125449.